Breakage Behavior Characterization of Micron-Scale Particles

I. Livk and D. Ilievski
Parker Cooperative Research Centre for Integrated Hydrometallurgy Solutions, CSIRO Minerals, Bentley, WA 6982, Australia

DOI 10.1002/aic.11135
Published online February 28, 2007 in Wiley InterScience (www.interscience.wiley.com).

A method for quantitative characterization of breakage of particulate material is presented. The approach developed uses a 3-D population balance (PB) breakage model, which describes the changing population of particles in a "origin-size-toughness" domain, to extract breakage parameters from dynamic tracer and size evolution experimental data. The breakage behavior is captured in terms of the model parameters of breakage rate and breakage distribution function. It is shown that utilization of the dynamic tracer distribution information contributes significantly to the accuracy and robustness of the breakage parameter estimation. The method is validated by demonstrating good agreement of the model with measured dynamic particle size distributions and tracer distributions. It is also demonstrated that the 3-D PB breakage model better captures the highly distributed nature of the dynamic experimental data than an equivalent 2-D model. The usefulness of the technique for characterization of breakdown characteristics is demonstrated using commercial aluminium oxides; both for quantitatively differentiating the breakage behaviors and also for providing insights into the fundamentals of the breakage mechanisms. "Breakage maps" and "breakage activity" plots are introduced as useful formats for presenting the complex breakage information. © 2007 American Institute of Chemical Engineers *AIChE J,* 53: 780–792, 2007
Keywords: particle strength, particle breakage, breakage rate, multidimensional population balance, particle toughness, alumina

Introduction

The breakage of micron-scale particles (i.e. 1–500 μm) is an important phenomenon that takes place in a variety of industrial unit operations. In some cases it is desirable, e.g. comminution in mineral processing operations for the purpose of liberating the valuables from the matrix. In other cases it is undesirable; e.g. in alumina calciners it results in product loss, decline in product quality, increased environmental, and health hazards. To control the breakage of particulate material it is first necessary to quantify the distributed breakage behavior in terms of the basic rate processes.

Most mathematical modeling of breakage processes in commercial multiphase unit operations has focused on identifying breakage laws common to a wider population of particles, rather than a stochastic approach describing the interactions of each particle; though the results from the two approaches converge for linear systems in the limit for large simulations.

The population balance (PB), given by Eq. 1, represents a convenient mathematical framework for modeling of breakage processes in this way.[1,2]

$$\frac{\partial n(\mathbf{x})}{\partial t} + \nabla \cdot \left(\mathbf{u}_{\text{ext}} n(\mathbf{x}_{\text{ext}})\right) + \nabla \cdot \left(\mathbf{u}_{\text{int}} n(\mathbf{x}_{\text{int}})\right) = (B - D) \quad (1)$$

Correspondence concerning this article should be addressed to I. Livk at iztok.livk@csiro.au.
Current address of D. Ilievski: Alcoa World Alumina, PO Box 161, Kwinana, Perth, Australia.

where $n(\mathbf{x})$ is the number density function, the vector of coordinates, $\mathbf{x}$, consists of the external, $\mathbf{x}_{ext}$, and internal, $\mathbf{x}_{int}$, coordinates. Vector $\mathbf{u}$ represents the velocities with respect to different coordinates. B and D are the birth and death processes associated, in this case, with particle breakdown. The widely used breakage equation given by Eq. 2[1,3] is a simplification of Eq. 1 that describes particle breakage dynamics in uniform, one-dimensional space, i.e. particle size (v) as the internal coordinate.[2] B and D are expressed in terms of a time independent breakage rate, S, and breakage distribution function, b, which describes the number distribution of particles resulting from the breakage of a parent particle, w.

$$\frac{\partial n(v,t)}{\partial t} = \int_v^\infty S(w)b(v,w)n(w,t)dw - S(v)n(v,t) \quad (2)$$

The first term on the RHS in Eq. 2 describes the flux of particles into the size interval v to $v + dv$ due to the breakage of all particles generated from the population of larger sized particles. The second term describes the flux out of this interval due to breakage. As will be demonstrated below, the highly distributed nature of particulate materials limits the usefulness of such simplified one-dimensional PB breakage equation models. Similarly, Pearson et al.[4] found that more internal coordinates are usually required to model granulation processes. Indeed, the use of multi-dimensional PB to model particulate systems with respect to coordinates other than particle size is becoming more common.[2,5–9]

In this work, a 3-dimensional dynamic PB breakage model is formulated and then utilized to quantitatively characterize the breakage of two different commercial aluminium oxide samples. Precise and sophisticated experimental breakage data were necessary for estimation of the breakage model parameters to avoid issues with over parameterization and ill-conditioning, well documented problems associated with modeling and parameter estimation in complex systems.[2,10,11] The experimental information used included measurements of the evolving particle size distributions and various tracer element distributions with respect to time and size. Validation of the model predictions is also presented. Figure 1 illustrates the methodology used to investigate the breakage behavior. Breakage parameters were estimated by solving an inverse problem, with the model parameters set such to achieve best match between the model prediction and experimental data. These quantitative estimates of the breakage parameters were used to identify the breakage mechanism, enabling a quantitative comparison of breakage of different samples. Because of the distributed nature of the breakage data breakage maps and breakage activity plots are introduced to help visualize the breakage model results. The important additional information provided by the tracers was obtained using a modification of the novel alumina doping method developed by Clerin and Laurent,[12] who used this information to quantitatively differentiate breakage behavior of different alumina samples. They did not use the time dependent tracer and PSD information for parameter estimation or modeling of alumina breakage, using instead a single dimensional mass balance-based breakage model.

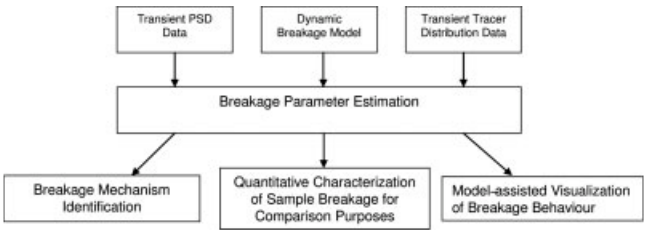

Figure 1. An overview of the methodology used to quantitatively characterize particle breakage behavior.

The Breakage Model

Population balance breakage model formulation

The multidimensional PB breakage model formulated here extends on the concept by Hounslow et al.,[6] who used a two-dimensional PB to model a population of granules distributed with respect to size and origin. To get agreement between their experimental data and model they also introduced time dependency into the breakage rate term, i.e. a decrease in the breakage rate with time. This time dependent behavior has been widely reported in the literature[6,13–15] and has also been observed in our laboratory attrition experiments with various micron-sized powders, which showed that the rate of new particle generation during attrition decreases with time despite the continued presence of some larger particles.

The changing breakage behavior can be explained as a result of either changes in the breakage resistance of particles with time spent in the breakage environment, or changes in the breakage environment, e.g. as the particle size changes.[14] A number of mechanisms that result in the toughening of brittle materials have been described in the literature, e.g. crack-tip-shielding mechanisms.[16] In general, these postulated mechanisms act by either increasing resistance to crack propagation or reducing crack energy. Other mechanisms are postulated to weaken a particle with time, e.g. fatigue. A simpler alternative explanation for this observation is that the easier to break structures in the sample are broken first, leaving behind particles of varying strength, but stronger on average and, hence, decreasing the opportunities for breakage with time. In the case of the alumina test system used here, this picture of particle breakage behavior is further complicated by the great heterogeneity in size, external and internal structure arising from the complex sequence of stages involved in manufacture, e.g. complex seeding strategies, agglomeration, cementation, nucleation, and a complicated thermal decomposition stage involving anisotropic shrinkage. This heterogeneity, overlayed by any progressive "toughening" or "weakening" mechanisms results in a population, which in a given breakage environment is distributed with respect to "resistance to further breakage" or toughness, as well as by other dimensions such as size and origin.

The size and origin dimensions have been previously used in modeling of breakage processes[6]; the approach adopted here to deal with the distributed breakage nature was to introduce a third internal coordinate into the breakage PB equation to represent "toughness". The particle "origin" coordinate, i.e. the size of the parent particle from which a daughter particle has been generated, and the "size" coordinate, represent-

ing the current size of a particle, are simple to conceptualize and can be readily measured (although several different particle size dimensions can be defined for irregular-shaped particles). The toughness coordinate is more challenging. First, numerous terms and definitions exist for this property, such as fracture stress, failure stress, fracture toughness, strength, attrition resistance, etc. Secondly, the measurement of various "toughness" properties of individual irregularly shaped, micron-sized particles can be very difficult. Although techniques do exist, such as nanoindentation tests and single particle impact tests, the analysis of sufficient numbers required to characterize a population is very time consuming and the authors are not aware of any commercial bulk analyses techniques that report distributed "toughness" values, such as analogous to the deconvolution techniques used by some particle size analysis instruments. These complications were handled here by treating the time spent by a particle in the breakage environment without breaking, τ, as a proxy measure for the toughness state variable. Populations characterized by a larger value of τ comprise of particles that have not experienced a breakage event for a longer period suggesting overall higher breakage resistance or toughness.

The particle breakage process is then modeled by Eq. 1, with the state of the particle population during a breakage experiment determined by the number density function distributed with respect to the particle origin (λ), size (v), and toughness (τ)

$$n(\mathbf{x}_{\text{int}}) = n(\lambda, v, \tau, t) \tag{3}$$

The proposed model views the breakage process as a collection of events averaged over the volume of the attrition apparatus. The assumption of spatial uniformity negates the need for the second term on the LHS of Eq. 1, which contains external coordinates. Linear breakage is also assumed, i.e. the breakage behavior of a particle is not affected by the state of the population as a whole. Despite these simplifications, the model is still very complex and further simplification was achieved by reducing the overall dimensionality of the problem. This was done by modeling the distribution of particles w.r.t. the origin coordinate, λ, using a piece-wise formulation for Eq. 3. In this approach, components of a joint marginal number density distribution, w.r.t. the particle size and toughness coordinates, are calculated separately for a series of parent particle size intervals, as indicated in Eqs. 4 and 5.

$$n(\lambda, v, \tau, t) \approx \begin{cases} n_1(v, \tau, t) & \lambda_2 \le \lambda \le \lambda_2 \\ n_2(v, \tau, t) & \lambda_2 \le \lambda \le \lambda_3 \\ \cdot & \\ \cdot & \\ n_h(v, \tau, t) & \lambda_h \le \lambda \le \lambda_{h+1} \end{cases} \tag{4}$$

where h is the number of parent-particle size intervals. Individual components of the piece-wise number density function are defined as

$$n_l(v, \tau, t) = \int_{\lambda_l}^{\lambda_{l+1}} n(\lambda, v, \tau, t) d\lambda \tag{5}$$

The 3-D breakage equation can now be converted into a set of 2-D PB equations, in terms of $n_l(v,\tau, t)$ for each parent particle size interval, by appropriately modifying the convective term on the LHS and the birth and death term on the RHS of Eq. 1. The first term is modified to account for the particle toughness distribution as

$$\nabla \cdot \left(\mathbf{u}_{\text{int}} n(\mathbf{x}_{\text{int}})\right) = \frac{\partial}{\partial \tau}\left[u_\tau n_l(v, \tau, t)\right] \tag{6}$$

Noting that toughness, τ, is defined as the time particles spend without breakage, then,

$$u_\tau = \frac{d\tau}{dt} = 1 \tag{7}$$

The birth and death terms in Eq. 1 are substituted by a breakage equation (Eq. 2), modified here to incorporate the toughness internal coordinate, giving

$$\frac{\partial n_l(v, \tau, t)}{\partial t} = -\frac{\partial n_l(v, \tau, t)}{\partial \tau} + \delta(\tau - \tau_0) \times \int_v^\infty \int_{\tau_0}^{\tau_m} b(v, w) S(w, \tau) n_l(w, \tau, t) d\tau dw - S(v, \tau) n_l(v, \tau, t) \tag{8}$$

where the breakage distribution function, $b(v,w)$, describes the number density distribution of fragments produced upon breakage of a particle size w. $S(w,\tau)$ is the specific breakage rate of particles dependent on the size and toughness state. The breakage distribution function is assumed to depend only on size, otherwise the complexity of the model and experimental information required for the model identification increases dramatically. The first term on the LHS of Eq. 8 describes the rate of accumulation of particles within the joint v to $v + dv$ size and $\tau + d\tau$ toughness state interval. The changes to this joint interval occur as a result of either breakage events or reclassification with respect to toughness, resulting from continued survival without breakage. The first term on the RHS represents the net rate of toughness reclassification for particles remaining in the v to $v + dv$ size interval. The second term on the RHS denotes the flux of particles into the size interval v to $v + dv$ due to the breakage of particles from the population of larger sized particles of any toughness state. The third term describes the removal of particles due to breakage. Alternatively, Eq. 8 could be reformulated by dropping the second term on the RHS, and stating the boundary condition for $n_l(v,\tau_0,t)$ as the double integral without the Dirac delta function. This approach is similar to the PB formulation of Shah and Ramkrishna[17] for droplet dispersions.

The model's treatment of the toughness state variable, though consistent with how it was defined as a proxy for toughness, shows that τ does not necessarily represent the true or underlying "toughness" of an individual particle. However, it is postulated, following the reasoning of Haseltine et al.[18] and Ramkrishna[2] that for a large particle population with τ small compared with the time periods over which measurable differences in the PSD occur, τ represents a plausible relative measure of the average "toughness" of that population of particles. The Dirac delta function term, $\delta(\tau - t_o)$ in Eq. 8, reassigns all freshly broken particles into the minimum toughness interval. This was introduced to capture the postulate, based on scanning electron microscopy (SEM)

images of attrited alumina particles, that many of the recently broken particles will be more prone to breakage because of the shape irregularities arising from the breakage and due to their history (i.e. something about them has caused them to break recently). As is demonstrated later by the agreement between the model prediction and experimental data, this hypothesis is reasonable for the alumina system. However, it is acknowledged that different particulate systems may exhibit different behavior.

Breakage parameters and constitutive equations

The breakage parameters are introduced into the breakage model via the constitutive equations used to model the breakage rate, S, and the breakage distribution function, b. $S(v,\tau)$ is expected to be a function of the material's mechanical properties, structural properties, size, the threshold impact energy required for damage to the particle, and the mass specific energies to which the particles are being exposed. Some workers have proposed that S also depends on the state of the other particles comprising the population, i.e. nonlinear breakage kinetics.[19,20] Linear breakage kinetics are assumed here. It is also assumed that all relevant variations in the material properties and structural properties, including the threshold energy, are captured by the toughness state variable, τ.

In this work, the size dependency in S is modeled by a power law relationship, following Hill and Ng[3] and others,[7] who report that this widely used form is a reasonable representation of experimental breakage data. Clerin and Laurent[12] used a power law correlation for the alumina system, in a single dimensional mass-based breakage model following Epstein.[21]

Toughness dependency is introduced into the breakage rate equation to describe the decreased probability for breakage for tougher particles, and is modeled by a first order process. Separate breakage rate functions were used for the original parent population, S_p, and the for the daughter particles, S_d. The reasoning being that the parent particles, e.g. commercial alumina particles, are engineered to resist breakdown and attrition, whereas the structure of the daughter fragments produced upon breakdown cannot be controlled and can take on a wide range of different forms. These forms may include structures that make them easier to break further, e.g. sharp corners, or they may be tougher, e.g. rounded corners or because the easy to break structures are gone. SEM images show significant differences in the respective morphologies of the daughter and parent particles. It was also observed that better fits to the experimental breakage data were obtained when separate functions were used.

The breakage rate function used for the daughter particles, combining the power law size dependency, and the first order toughness relationship, takes the form

$$S_d(v,\tau) = S_{c,0} \cdot e^{-\tau/\tau_c} \cdot \left(\frac{v}{v_f}\right)^{\eta} \tag{9}$$

where v_f is the maximum particle size. $S_{c,0}$ and η are the daughter particle breakage rate parameters and incorporate information on the particle properties and the breakage environment. τ is the toughness introduced above and the constant, τ_c, defines how rapidly the daughter particle breakage rate decreases with respect to the toughness coordinate. It is most likely a measure for how rapidly the weaker structures in the sample are broken. The model assumes that τ_c is the same for all particles for simplicity. Equation 9 describes an average breakage rate of the population of particles of state (v,τ) and not single particle behavior, which would be stochastic in nature.

The parent particle breakage rates were modeled using the following empirical relationship

$$S_p(\lambda,\tau) = \left(p_1 + p_2 \cdot \left(\frac{\lambda}{\lambda_f}\right) + p_3 \cdot \left(\frac{\lambda}{\lambda_f}\right)\right) \cdot e^{-\tau/\tau_c} \tag{10}$$

Equation 10 was identified by trial and error and found to be a good compromise between a flexible functional form able to describe a range of experimental breakage rate data and the number of parameters. A number of functional forms were trialed, including Eq. 9, however, more work is needed to establish a phenomenological understanding for this relationship. The parameters p_1 to p_3 incorporate information on the parent population properties and the breakage process conditions. Again for simplicity and in the absence of contradictory findings, the constant τ_c is assumed to be the same for all particles. In the discretized form of the PB breakage model, introduced below, parent particles are defined as the particles that remain in the original size interval.

The breakage distribution function, $b(v,w)$, is the number of particles sized v to $v + \mathrm{dv}$ arising from breakage of a particle sized w. The function is subject to the constraints of volume conservation, symmetry, and the total number or normalization condition.[2] Various empirical models for the breakage function have been published; some underpinned by physical reasoning, e.g. parabolic functional form to describe attrition processes. The breakage distribution function model used here is based on Hill and Ng.[22] They developed a method for modeling the breakage distribution function for multiple breakage event processes in terms of a joint probability function expressed as either the summation or product of power laws. In the case of binary breakage, thus subject to the constraint

$$\int_0^w b(v,w)dv = 2 \tag{11}$$

and using their summation formulation, gives

$$b(v,w) = \frac{m+1}{w^{m+1}}[v^m + (w-v)^m] \tag{12}$$

where m is the breakage distribution function parameter. This simple, one-parameter model has the flexibility to describe different breakage mechanisms. This is illustrated in Figure 2 using three different values for the parameter m and showing that for high values of m the breakage behavior is more attrition-like, whereas for low values the breakage behavior is more fracture-like resulting in the formation of more equisized particles.

Solution of the breakage model

Equation 8 is too complex to solve analytically for cases of interest and needs to be transformed appropriately for nu-

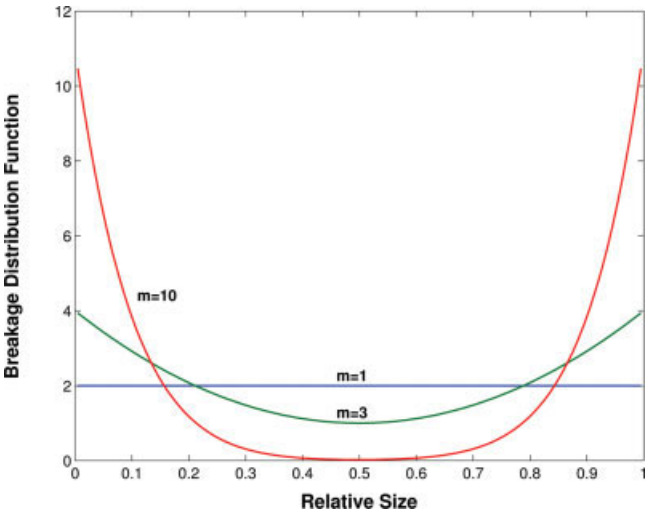

Figure 2. Number-based power-law breakage distribution function for different values of parameter *m*.

[Color figure can be viewed in the online issue, which is available at www.interscience.wiley.com.]

merical solution. This was done by discretization of the continuous PB in Eq. 8, which converts it into a system of ODEs that can be solved using standard numerical techniques. In the descretized form, the particle population for a given parent particle size, l, is represented by a set of particle numbers in a discrete size-toughness region, $N_{ik,l}$, which is related to the number density by the following equation

$$N_{ik,l} = \int_{v_i}^{v_{i+1}} \int_{\tau_k}^{\tau_{k+1}} n_l(v,\tau,t)\,dv\,d\tau \tag{13}$$

where v_i, v_{i+1}, τ_k, and τ_{k+1} represent the boundaries of a size-toughness region, as shown in Figure 3.

To derive the discrete form of the breakage model, the first term on the RHS of Eq. 8, the convective term with the unity velocity, has been discretized using a simple finite difference approximation, while the second term has been discretized in accordance with the discretization of Hill and Ng[3] to yield the following discretized breakage model

$$\begin{aligned}\frac{d}{dt}N_{ik,l}(t) &= H(\bar{\tau}_k-\bar{\tau}_1)\frac{N_{ik-1,l}(t)}{\tau_k-\tau_{k-1}} - \frac{N_{ik,l}(t)}{\tau_{k+1}-\tau_k} \\ &+ \delta(\bar{\tau}_k-\bar{\tau}_1)\sum_{k=1}^{m}\sum_{j=i+1}^{n}\beta_j b_{ij} S_{jk} N_{jk,l}(t) \\ &+ \delta(\bar{\tau}_k-\bar{\tau}_1)\sum_{k=1}^{m}(1-\alpha_i)S_{ik}N_{ik,l}(t) - S_{ik}N_{ik,l}(t)\end{aligned} \tag{14}$$

where $N_{ik,l}(t)$ is the number of particles of size $\bar{v}_i$ and toughness $\bar{\tau}_k$ in the l-th parent size interval. b_{ij} is the discrete breakage distribution function and is obtained from Eq. 12, giving

$$\begin{aligned}b_{ij} &= \int_{v_i}^{v_{i+1}} b(v,v_j)\,dv = \frac{1}{v_j^{(m+1)}} \\ &\times \left(v_{i+1}^{m+1} - v_i^{m+1} + (v_j - v_i)^{m+1} - (v_j - v_{i+1})^{m+1}\right)\end{aligned} \tag{15}$$

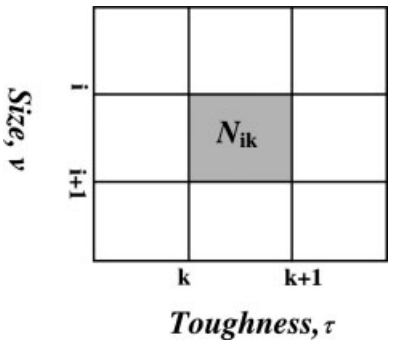

Figure 3. Particle number in a discrete size-toughness domain.

$H(\bar{\tau}_k - \bar{\tau}_1)$ and $\delta(\bar{\tau}_k - \bar{\tau}_1)$ are the Heaviside step function and the Dirac delta function acting at τ greater than and equal to $\bar{\tau}_1$, respectively. β_j and α_i are additional probability functions, as derived by Hill and Ng,[3] introduced to ensure correct prediction of total particle number and conservation of total particle volume by the discretized breakage equation. The first two terms on the RHS of Eq. 14 represent the net change in numbers in joint interval due to toughness reclassification for particles not experiencing a breakage event with time. The third and fourth terms account for the increase in particle numbers due to the incoming particles generated by the breakage of the particles of equal or larger size. Both terms are nonzero only for the minimum toughness interval, $\bar{\tau}_1$. The last term accounts for the loss of particles from the ik-region due to breakage. Because of the finite number of discrete size intervals, the rate of generation of new particles from the smallest size interval is zero. The characteristic size and toughness of discrete intervals are defined as

$$\bar{v}_i = \frac{v_i + v_{i+1}}{2} \tag{16}$$

$$\bar{\tau}_k = \frac{\tau_k + \tau_{k+1}}{2} \tag{17}$$

Similarly, the characteristic size of a parent size interval is

$$\bar{\lambda}_l = \frac{\lambda_l + \lambda_{l+1}}{2} \tag{18}$$

The model in Eq. 14 represents an initial value problem, which was solved using an explicit Runge–Kutta (2,3) formula, as implemented by the "ode23" function in MATLAB[23] computational environment. Note that to determine the piece-wise solution of the particle population distribution w.r.t. all three coordinates, the system of discretized equations presented in Eq. 14 is solved separately for each parent size interval, as indicated by Eq. 4. The initial conditions used for each parent size interval, $\bar{\lambda}_l$, are given as

$$\mathbf{N}(\bar{\mathbf{v}},\bar{\tau},0) = \begin{bmatrix} \delta(\bar{v}_1-\bar{\lambda}_l)\cdot N_1(0) & 0 & \cdots & 0 \\ \delta(\bar{v}_2-\bar{\lambda}_l)\cdot N_2(0) & 0 & \cdots & 0 \\ \vdots & \vdots & & \vdots \\ \delta(\bar{v}_n-\bar{\lambda}_l)\cdot N_n(0) & 0 & \cdots & 0 \end{bmatrix} \tag{19}$$

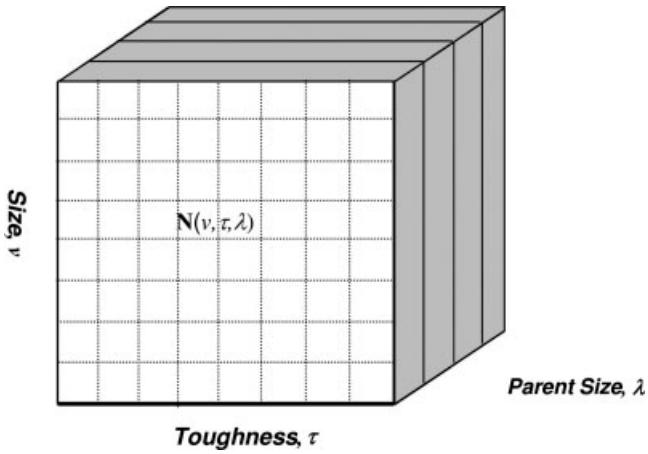

Figure 4. Presentation of the information generated by the breakage model.

where $\mathbf{N}(\bar{\mathbf{v}}, \bar{\tau}, 0)$ is the matrix of values of $N_{ik,l}$ at $t = 0$ for parent size $\bar{\lambda}_l$, $\delta(\bar{v}_i - \bar{\lambda}_l)$ is the Dirac delta function acting at the size equal to the respective parent size, and the elements N_i are the numbers of particles of size $\bar{\mathbf{v}}_i$. The initial value matrix shown is valid for the case where $\bar{\mathbf{v}}$ and $\bar{\boldsymbol{\lambda}}$ are the same vectors. Note that in this case the matrix first column has only one nonzero element, with all the other elements equal to zero.

The information generated by the dynamic breakage model, at a given time instant, can be presented schematically as shown in Figure 4, where the three-dimensional particle space, $\mathbf{N}(v,\tau,\lambda)$, is represented by a cube. Each slab in this cube represents the particle size-toughness distribution resulting from a given parent particle size interval.

The advantages of the finite difference discretization technique used in this work are its implementation ease and robustness within iterative optimization loops. However, it results in a relatively large set of ordinary differential equations to achieve the desired solution accuracy. In our case, the total particle volume was conserved with a tolerance better than 0.1%. A small discrepancy in the model predicted volume consistency is ascribed to the fact that the size domain is finite—it does not go down to zero size. Other numerical techniques that could also be used include: collocation methods,[24] method of characteristics,[25] or high-resolution schemes of Ma et al.[26]

Estimation of Breakage Parameters

The breakage parameters were estimated such that the deviation between the experiment and model prediction was minimized. Such inverse breakage problems can be ill-conditioned[2]; the inclusion of the tracer distribution data and specification of the functional forms for the constitutive equations in the present case imposes additional constraints on the solution and increases the robustness of parameter estimation procedure. The tracer distribution data provide direct information on breakage distribution function. The use of tracer information in determination of breakage parameters is discussed in a considerable depth in the paper by Gardner and Sukanjnajtee.[27] In their work, the authors anticipated a tracer method that would use a number of tracers simultaneously, which is exactly the approach implemented in the present work. The estimation problem in our case can be stated as

$$\begin{array}{ll} \min\limits_{\theta} & \Phi(\mathbf{N}(t),\theta) \\ \text{subject to} & \text{Breakage Model} \end{array} \tag{20}$$

where the objective function, Φ, includes two terms, one for the PSD and the other for the tracer distribution (TRD) as

$$\Phi(\mathbf{N}(t),\theta) = \Phi_{\text{PSD}} + \Phi_{\text{TRD}} = \sum_{i=1}^{n}\sum_{s=1}^{\mu} \omega_i (N_{i,s}^{\text{exp}} - N_{i,s}(\theta))^2 + \sum_{q=1}^{Q}\sum_{z=1}^{Q}\sum_{s=1}^{\mu} \psi_q (X_{q,z,s}^{\text{exp}} - X_{q,z,s}(\theta))^2 \tag{21}$$

The set of breakage parameters, θ, is

$$\theta^T = [S_{c,0}\ \eta\ p_1\ p_2\ p_3\ m\ \tau_c] \tag{22}$$

$N_{i,s}^{\text{exp}}$ and $N_{i,s}(\theta)$ are the experimental and model predicted number of particles in the ith size interval at the sth time instant, respectively. Similarly, $X_{q,z,s}^{\text{exp}}$ and $\mathrm{X}_{q,z,s}(\theta)$ are the experimental and model predicted mass fractions of the q-tracer doped particles appearing in the zth size interval at the sth time instant, respectively. Note: the size intervals for the experimental PSD data are determined by Coulter Counter Multisizer, and for the tracer distribution data by sieving (both q and z). The model predicted qth tracer mass fraction transferred to the zth size interval at the sth time instant, $X_{q,z,s}$, can be calculated from the set of individual parent-size fractions, $N_l(v,\tau,t)$, assuming a constant solids density using the following relationships

$$X_{q,z,s} = \frac{\bar{v}_z \sum\limits_{k=1}^{K}\sum\limits_{l=q-}^{q+} N_l(\bar{v}_z, \bar{\tau}_k, t_s)}{\sum\limits_{i=1}^{h}\left(\bar{v}_i \sum\limits_{k=1}^{K}\sum\limits_{l=q-}^{q+} N_l(\bar{v}_i, \bar{\tau}_k, t_s)\right)} \tag{23}$$

where q^- and q^+ denote the index corresponding to the lower and upper boundaries of the qth tracer size fraction.

The experimental value of q-tracer mass fraction, $X_{q,z,s}^{\text{exp}}$, is simply obtained as a ratio between the experimentally determined mass of particles doped by the qth tracer, $M_{q,z,s}$, and total mass of particles in the zth size fraction, $M_{z,s}$, as

$$X_{q,z,s}^{\text{exp}} = \frac{M_{q,z,s}}{M_{z,s}} \tag{24}$$

The weighting factors, ω_i and ψ_q in Eq. 21, are set so that the sensitivity of the objective function is balanced with respect to both terms. Although the weights can be used to incorporate information on the measurement error, in this case they were only used for scaling the measurements of different dimensionality and their best values were determined by trial and error, as is commonly done for cases where replicate experiments to assess data error structure are not available.[28] In our case, ω_i equals to 100 $\bar{v}_i$, and ψ_q is unity for all q. The breakage parameters were determined by the solution of the nonlinear optimization

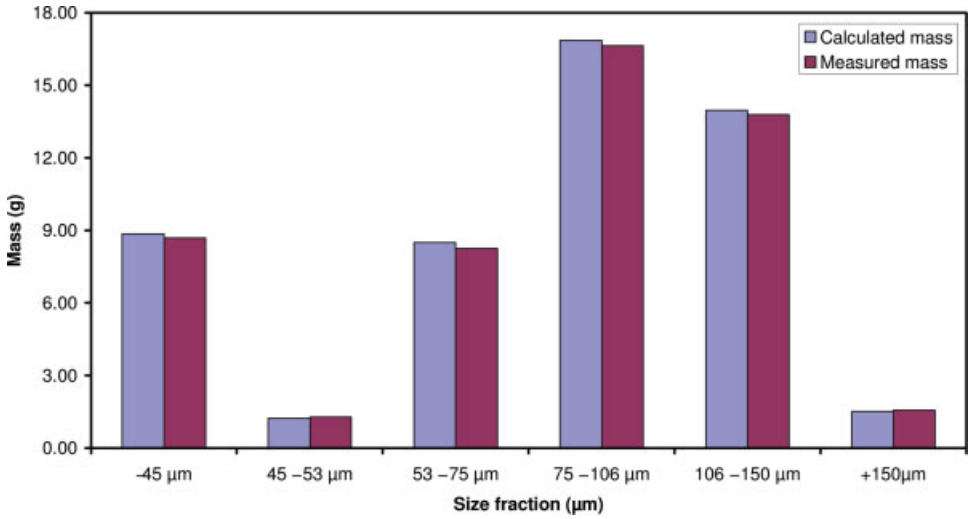

Figure 5. Uniformity of the dopant distribution demonstrated by comparison of the measured and calculated mass of the dopant in each size fraction after 15 min attrition.

[Color figure can be viewed in the online issue, which is available at www.interscience.wiley.com.]

problem stated in Eq. 21, carried out using a direct search method available within the MATLAB Optimization Toolbox.[29] Configuration parameters of the MATLAB direct search procedure, for example tolerances on the objective function and parameter values, were set such to ensure convergence of all breakage parameters. This was checked by inspecting the evolution of breakage parameter values and values of the objective function during a complete optimization run.

Experimental Procedures

The quantitative method described above has been used to characterize the breakage behavior of about 15 aluminium oxide samples to date. The results for two different aluminium oxide samples, denoted Sample A and Sample B, are reported here to demonstrate the technique. These were derived from commercial aluminium trihydroxides obtained from different alumina refineries and calcined under identical conditions to the oxide form.

Prior to each attrition test, the material was dry sieved and separated into six size-fractions. Particles from each size-fraction were doped with a different tracer element following the procedure developed by Clerin and Laurent.[12] The doping elements were Mo, Co, Cu, Cd, and Zn. The undoped particles represent the sixth fraction. The imbibing process is aided by the very porous character of commercial grade alumina particles $\sim$80 m^2/g.

A number of tests were conducted to demonstrate that the doping did not significantly change the character of the alumina. Analyses of the alumina phase compositions of doped and undoped alumina samples, using the method described by Whittington and Ilievski,[30] showed no significant differences in the relative amounts of χ, γ, θ, κ, and α phases. Tests, looking at the rate of particle number generation and measured by Coulter Counter, showed no significant differences between doped and undoped samples. The uniformity of dopant distribution was tested by (1) preparing a doped narrow size fraction and measuring the concentration of dopant, (2) attriting that size fraction, (3) sizing the attrition product, (4) classifying the attrition product into different size fractions and analyzing each fraction by ICP for the dopant, and finally, (5) checking that the dopant proportions were uniformly distributed across the resultant size fractions. The proportion of the dopant in each size fraction was constant to within experimental error, indicating uniform distribution. Figure 5 illustrates this result by comparing the actual mass in each of the size fractions after 15 min attrition with the amount calculated from the tracer composition data assuming uniform distribution of the dopant (Mo in this case).

The recombined sample is then subjected to the attrition process in a modified Forsythe–Hertwig spouted bed attrition device,[31] shown in Figure 6, for periods of time ranging from 1 to 15 min. After attrition, the solids were collected and sieved again into the original size fractions. A small portion of each size fraction was removed and submitted for the chemical analysis by ICP to determine size distribution of the tracer elements.

The particle size distributions (PSD) of the combined samples were measured with a Coulter Counter Multisizer IIe at each sampling instant. Measurements were made in duplicate to ensure repeatability and good mass recovery. Experimental data describing the evolution with time of the PSD and tracer distribution were used in the numerical part of the method to estimate breakage parameters for both samples.

Method Validation

The breakage model has been tested by assessing its ability to describe dynamic experimental data on:

1. Total number of particles,
2. Particle size distribution, and
3. Tracer fraction distribution with size.

Very good agreement between the model and experimental data has been observed for the 15 aluminium oxide samples

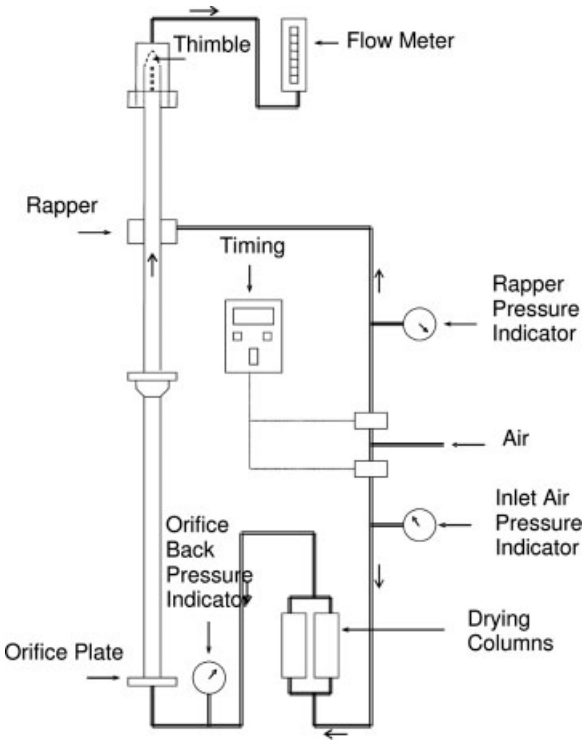

Figure 6. Forsythe–Hertwig attrition.

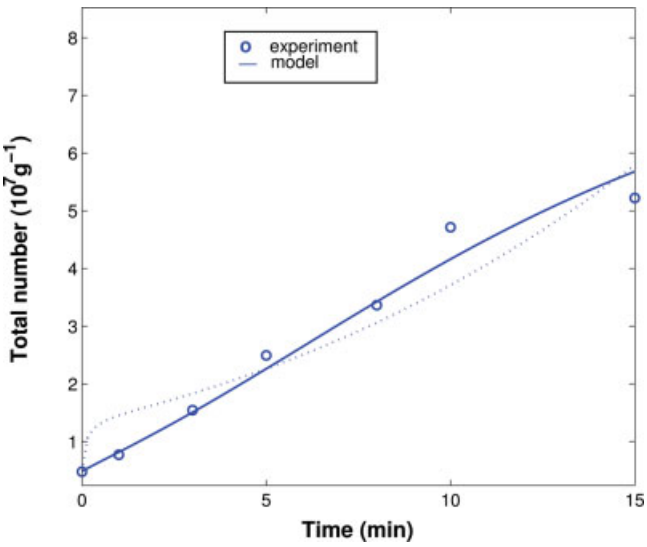

Figure 7. Evolution of the experimental and model predicted total number of particles during the attrition of Sample A.

The dotted line represents the prediction of a model that does not include the "toughness" coordinate. [Color figure can be viewed in the online issue, which is available at www.interscience.wiley.com.]

analyzed to date. The results of the validation tests for Sample A are presented for illustration. The results also demonstrate the benefit of the using the 3-D breakage model in the analysis, i.e. the addition of "toughness" as the third internal coordinate, versus an equivalent 2-D model that only includes size and parent size coordinates.

Figure 7 shows that the model predicted evolution of particle numbers is in good agreement with the measured values. It is clearly superior to the predictions made when the equivalent 2-D breakage model was used to estimate the breakage parameters from the data (i.e. the dotted line in Figure 7). However, it is noted that the agreement between experiment and 2-D model may improve if time dependent breakage parameter functions are used in the model.

A comparison between the experimental and model predicted volume-based PSDs at different time instants is presented in Figure 8. The PSD curves illustrate how the volume (mass) of material in the lower sizes increases due to breakage of larger particles. Note, the total volume of particles remains constant. As shown in the plot, the PSDs predicted by the model capture well the experimentally observed behavior.

Figure 9 presents the experimental and model predicted size distributions of the 75–106 μm tracer-doped particles after 15 min attrition. This size fraction contains the greatest mass. Note that at time zero, all of the mass was contained in the 75–106 μm size interval, and was at later times distributed to the lower size intervals due to breakage. The model satisfactorily predicts the experimentally observed final size distribution of doped particles, as shown in Figure 9. The small amount of the material predicted by the model in the size interval above the 75–106 μm size interval is a consequence of the numerical diffusion arising from the discretization. Also shown in Figure 9 (as a dotted line) is the tracer distribution predicted using the 2-D model for the breakage analysis. Clearly, the analysis using the 3-D breakage model better captures the experimental tracer distribution data.

Breakage Mechanism Identification

The breakage model was used to extract the breakage characteristics of samples A and B (i.e. breakage rate, break-

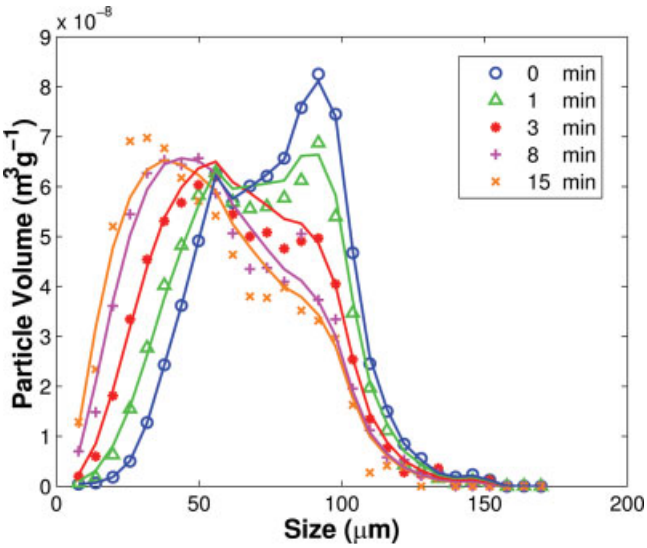

Figure 8. Experimental (symbols) and model predicted PSD (lines) at different times during the attrition of Sample A.

[Color figure can be viewed in the online issue, which is available at www.interscience.wiley.com.]

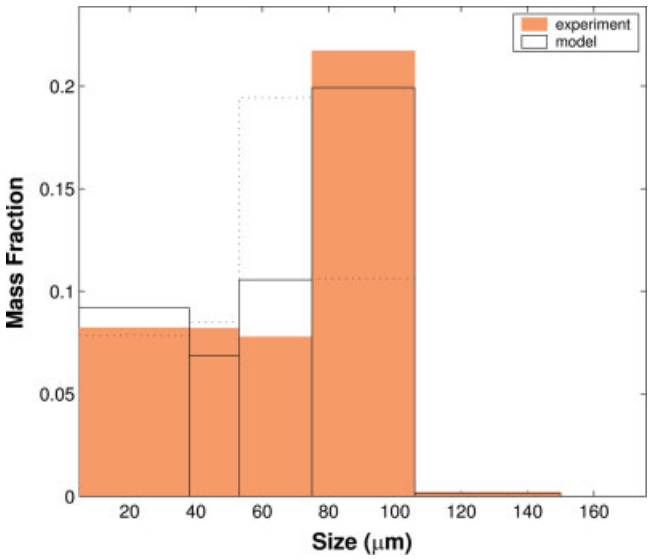

Figure 9. Experimental and model predicted size distribution of the 75–106 μm tracer doped particles after 15 min of breakage of Sample A.

The dotted line represents the prediction of a model that does not include the "toughness" coordinate. [Color figure can be viewed in the online issue, which is available at www.interscience.wiley.com.]

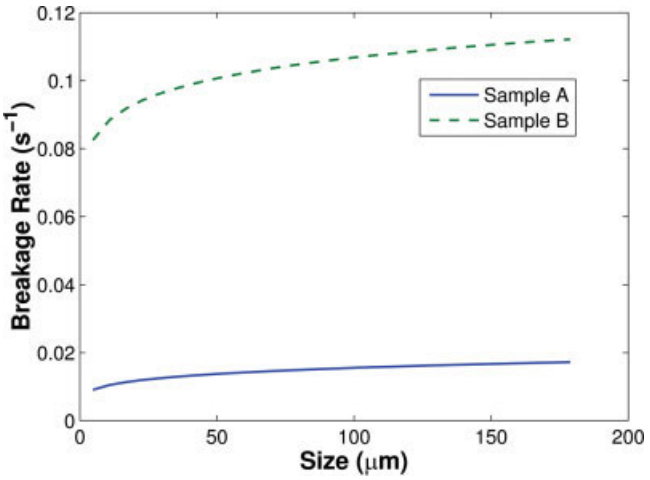

Figure 11. Daughter breakage rates estimated for Sample A and Sample B.

[Color figure can be viewed in the online issue, which is available at www.interscience.wiley.com.]

age distribution function) from the experimental dynamic PSD and tracer distribution data obtained using the attrition unit.

Figure 10 shows the parent breakage rate for both samples as a function of size. The parent breakage rates of both samples are very similar in magnitude and both exhibit a decrease with increasing parent particle size. This suggests that these materials either experienced some breakage prior to the experiments in the attrition tester and leaving only "resilient" particles in larger size fractions or were produced in a process that favors the formation of strong large particles. The latter is, indeed, the goal of most commercial Bayer operations for the production of alumina. It should also be noted that the uncertainty in the breakage rate estimates for sizes below 20 μm and above 120 μm are expected to be larger due to relatively small amount of material initially present in these regions.

The estimated daughter breakage rates are presented in Figure 11. In contrast to the parent breakage rates, the daughter breakage rates of both samples differ significantly, with Sample A exhibiting much lower values than Sample B. In both samples, the daughter breakage rates exhibit only a slight size-dependency.

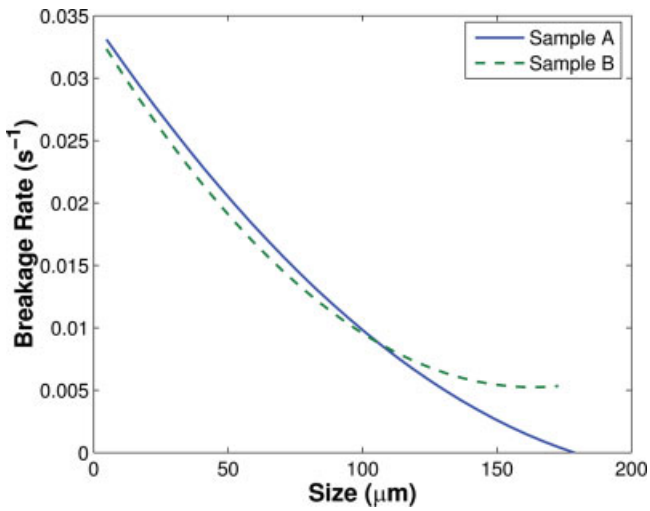

Figure 10. Parent breakage rates estimated for Sample A and Sample B.

[Color figure can be viewed in the online issue, which is available at www.interscience.wiley.com.]

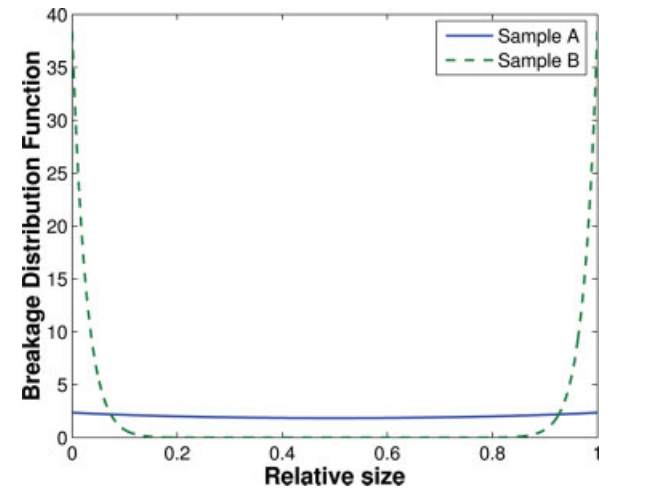

Figure 12. Estimated number-based breakage distribution functions of Sample A and Sample B.

[Color figure can be viewed in the online issue, which is available at www.interscience.wiley.com.]

Table 1. Estimated Values of Breakage Parameters

Sample	$S_{c,0}$	η	τ_c	m	p_1	p_2	p_3
A	0.017	0.059	124	1.4	0.035	−0.057	0.022
B	0.112	0.028	54	37.5	0.034	−0.063	0.035

For Sample A, parent and daughter breakage rates are of comparable magnitude, with differences between the two being more pronounced at the small and large size end, where uncertainties are higher. In the case of Sample B, the daughter breakage rates far exceed the parent particle breakage rates.

Figure 12 shows that the estimated breakage distribution functions for the two samples differ significantly. The breakage product from Sample A is distributed much more evenly by size than the breakage product resulting from sample B. These results suggest that the breakage mechanism of Sample A is more cleavage-like or fracture-like, while that of Sample B seems to be more attrition-like. The maximum breakage rates and breakage distribution functions presented for the two samples are obtained using the estimated values of corresponding breakage parameters, which are given in Table 1.

These postulated mechanisms are consistent with the breakage products observed in SEM images; Figure 13 shows both products after 10 min attrition in the attrition tester. Sample A appears to have more evenly sized particles, whereas Sample B has produced significant amounts of fine particles. SEM images of the initial samples show that they comprise mostly of large particles and contain few fines. Care is required in interpreting the images in Figure 13 due to issues with representative sampling and count statistics.

The quantitative breakage characteristics determined for these samples help to build a conceptual model of their respective breakdown behaviors and gives an insight into the possible internal structures that could explain the differences observed. First, that the parent particles have similar breakage rates is possibly due to both oxide samples having been being derived from aluminium trihydroxide particles produced in commercial operations that, although different, endeavor to produce a product of similar attrition resistance. The main difference between the samples appears to be that the daughter particles arising from Sample B are more rapidly broken down further to fines. This suggests a conceptual model of the initial daughter particles from Sample B as comprising of many easy-to-rupture structures, which result in the generation of a significant quantity of fines.

To help better visualize the breakage characteristics extracted from the data, the plots presented in Figures 14 and 15 show the number distribution of particles as a function of daughter and parent particle sizes for the sample A and B, respectively. The color spectrum is used as an indicator of particle numbers with red indicating the greatest numbers through to dark blue representing no particles. These "breakage maps" show the size distribution of daughter particles originating from a given parent size interval, as can be noticed by following the straight vertical line up from the diagonal. The parent particles, which at $t = 0$ represent the original sample, are depicted along the diagonal of a breakage map. The lower triangular part of a breakage map contains no particles (dark blue color), as none of the daughter particles can be larger than the parent. The breakage maps are generated from the data estimated by the dynamic breakage model, described above, using the breakage parameters extracted from the experimental data. Comparing these "breakage maps" at different time instants enables one to follow the evolution of newly generated particles originating from different parent particles.

Figure 14 shows that after 1 min of breakage of Sample A, most of the particles generated are only slightly smaller than the parents. At this stage, most of the daughter particles originated from the parents in the lower end of the parent PSD, where the numbers of parent particles and breakage rates are highest. After 15 min of breakage in the attrition device, the largest number of particles in the breakage product are newly generated fines (red color at the top) originating from parent particles sized around 40 μm.

In contrast to Sample A, the breakage maps for Sample B, shown in Figure 15, have a boomerang-like shape, which is consistent with the "attrition-like" breakage mechanism ascribed to Sample B based on the extracted breakage distribution function shown in Figure 12. The breakage map presentation can provide a distinctive fingerprint of a given material, which may prove to be a useful tool in comparison of breakdown behaviors of different materials.

Another useful format for visualization of breakage characteristics is the "breakage activity" plot, such as shown in Figure 16. These illustrate how the breakage activity is distributed with respect to size and time. Like breakage

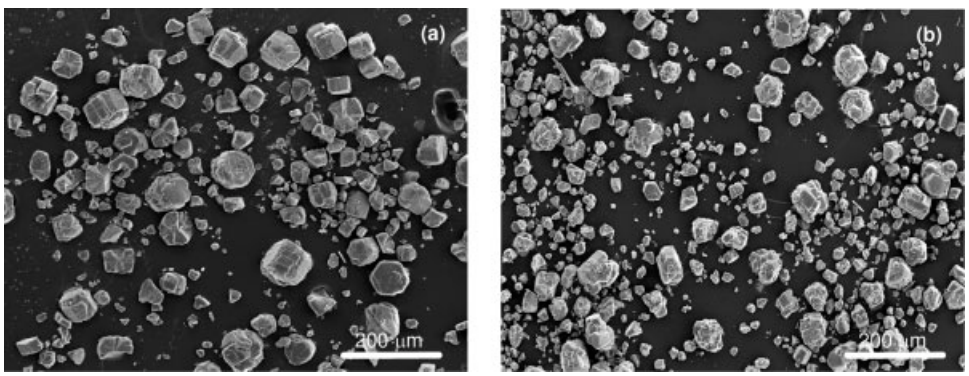

Figure 13. SEM images of the attrition products from Sample A (a) and Sample B (b) after 10 min in the attrition device.

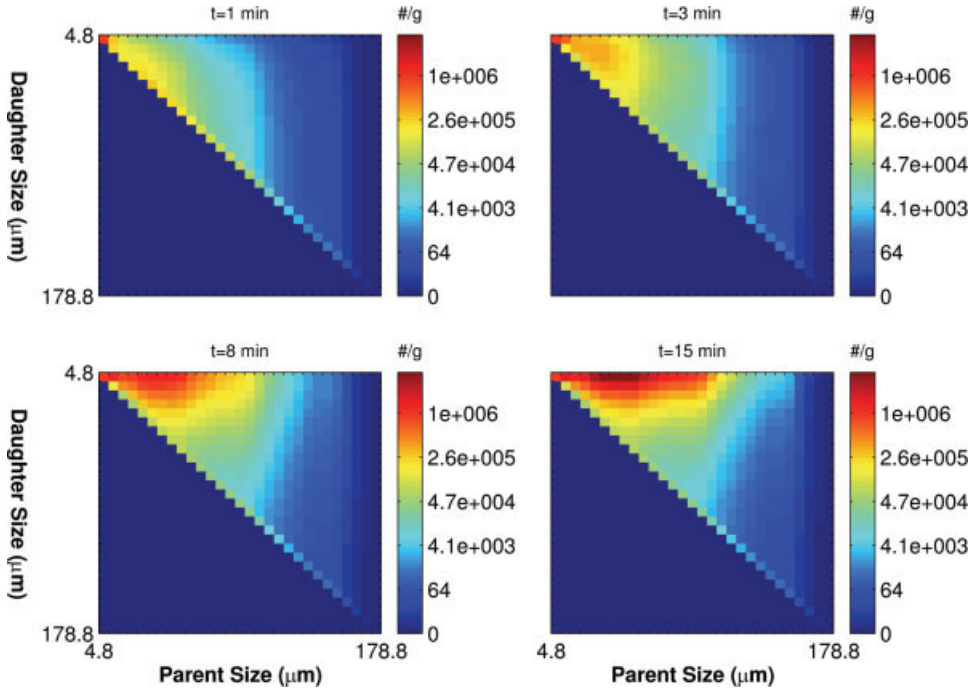

Figure 14. Model predicted number-based distribution of Sample A particles at four different time instants.

[Color figure can be viewed in the online issue, which is available at www.interscience.wiley.com.]

maps, breakage activity plots are generated from the dynamic PB breakage model. Figure 16 indicates that after 1 min of breakage the population of particles in Sample A has a wide spread of volume-based breakage rates with a maximum at the size of about 50 μm. After 2 min, the breakage activity increases in intensity and also starts propagating to smaller size intervals. The migration of breakage activity to smaller sizes continues until an external constraint, such as the size of smallest particle that can undergo break-up, is reached, e.g. the critical plastic deformation size limit. The overall breakage activity drops significantly at later times, as shown in the last plot of Figure 16, suggesting that most opportuni-

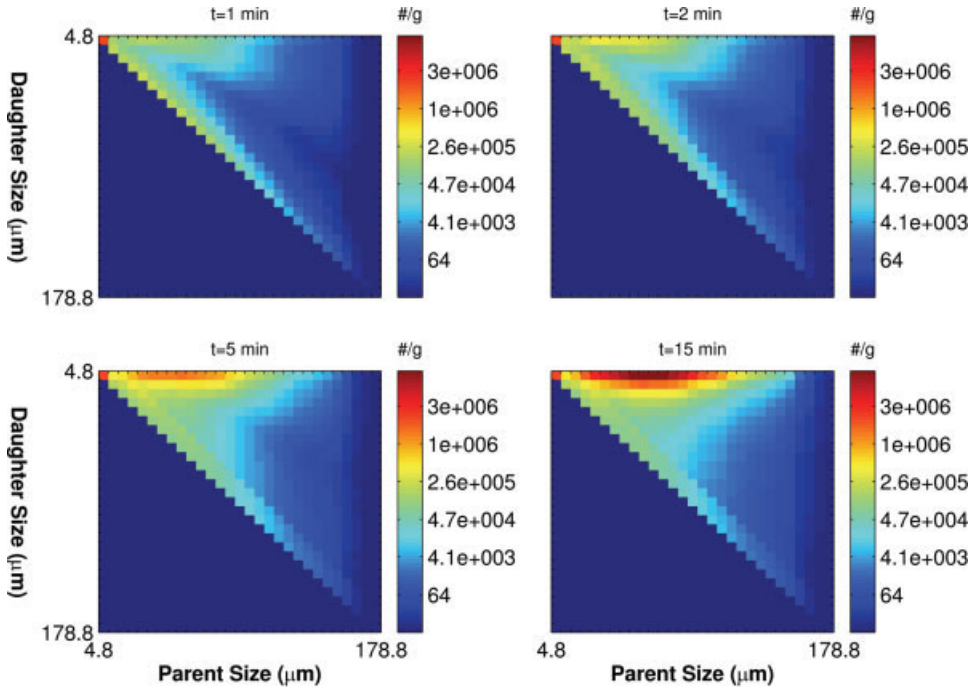

Figure 15. Model predicted number-based distribution of Sample B particles at four different time instants.

[Color figure can be viewed in the online issue, which is available at www.interscience.wiley.com.]

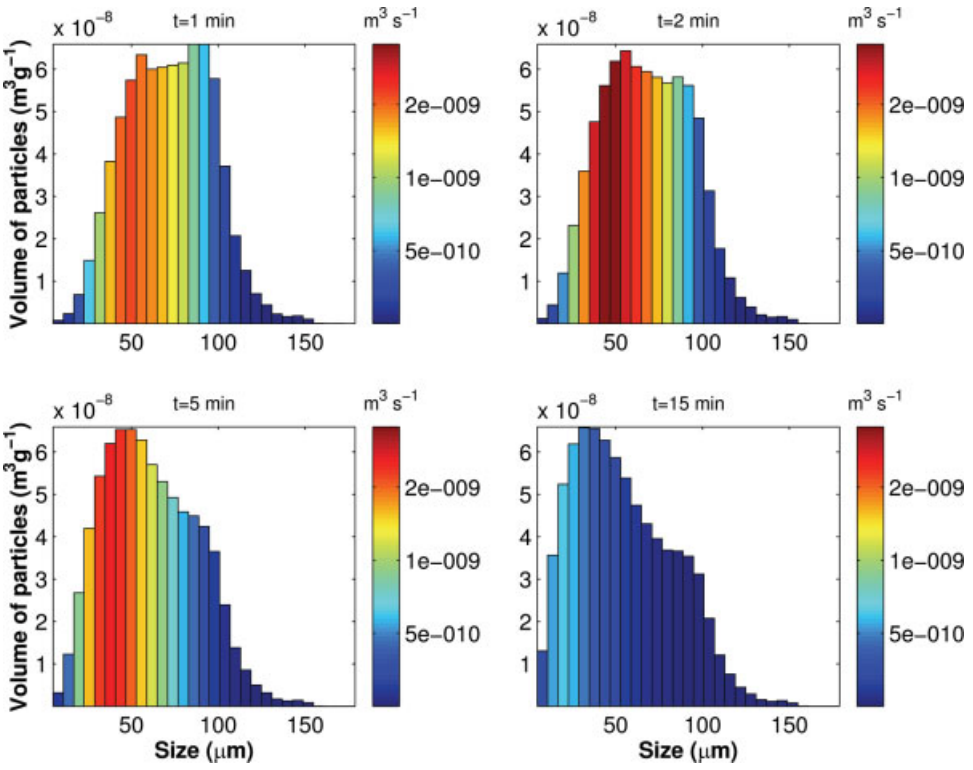

Figure 16. Model predicted volume-based breakage activity of Sample A at four different time instants.

[Color figure can be viewed in the online issue, which is available at www.interscience.wiley.com.]

ties for breakage have been exhausted in the given breakage environment. Note that the addition of toughness as the 3rd dimension in the PB breakage model has helped to capture this propagation of breakage activity behavior.

Conclusions

A novel method is presented, which combines experimental and numerical techniques for the quantitative analysis of breakage behavior. This method quantifies breakage parameters from transient experimental PSD and tracer distribution data using a three dimensional PB breakage model. A significant feature of the breakage model is that some of the time-dependent behavior of the breakage parameters is captured through a toughness state variable and the appropriate constitutive equations. The utilization of the tracer information in the method contributes significantly to the robustness of the breakage parameter estimation. The model-based analysis has been successfully validated by comparison to the experimental breakage product size distributions and tracer distributions.

The method's capabilities were illustrated by using it to quantitatively analyze the breakage characteristics of two aluminium oxide samples that had been prepared from aluminium trihydroxide product obtained from commercial Bayer plants. The resultant analyses clearly showed differences in the breakage behavior of the two samples and provided evidence for a phenomenological interpretation. The findings are consistent with the tracer results and SEM images.

The complex multi-dimensional information generated by the method is most clearly presented in the form of a "breakage map", which enables visualization of breakage variables distributed in two dimensions, and a "breakage activity plot", which shows the change in breakage activity with time for the whole population of particles.

Acknowledgments

The authors express their gratitude to the sponsors of the AMIRA 575A project, which has stimulated research innovation over a diverse range of areas. The sponsoring companies of this project were: Alcan, Alcoa World Alumina, Aughinish Alumina, BHP Billiton-Worsley Alumina, Comalco Aluminium, Hydro Aluminium, Outokumpu Technology, and Queensland Alumina. This research was supported by the Australian Government's Cooperative Research Centre (CRC) program via the Parker Centre for Integrated Hydrometallurgy Solutions. The authors thank Mark Schibeci for his significant contribution to the experimental work.

Notation

B = birth term, s^{-1}
D = death term, s^{-1}
K = number of toughness intervals
$M_{q,z,s}$ = mass of particles doped by a q-tracer in the sth size interval
n = number density
Q = number of sieving size intervals
P_1 = parent breakage rate constant, s^{-1}
$S_{c,0}$ = breakage rate constant, s^{-1}
t = time, s
$X_{q,z,s}$ = q-tracer mass fraction transferred to the zth size interval at the sth time instant

Greek letters

λ = parent particle volume, m^3
μ = number of time instants
θ = vector of breakage model parameters

τ = toughness state, s
τ_0 = minimum toughness, s
τ_m = maximum toughness, s
v = particle volume, m^3

Subscript

f = maximum size
i = size interval
k = toughness interval
l = parent size interval
q = tracer type
z = sieving size interval

Literature Cited

1. Randolph AD, Larson M. *Theory of Particulate Processes: Analysis and Techniques of Continuous Crystallization*, *2nd edition*. Toronto: Academic Press, 1988.
2. Ramkrishna D. *Population Balances: Theory and Applications to Particulate Systems in Engineering*. San Diego: Academic Press, 2000.
3. Hill PJ, Ng KM. New discretization procedure for the breakage equation. *AIChE J*. 1995;41:1204–1216.
4. Pearson JMK, Hounslow MJ, Instone T. Tracer studies of high-shear granulation. I. Experimental results. *AIChE J*. 2001;47:1978–1983.
5. Puel F, Févotte G, Klein JP. Simulation and analysis of industrial crystallization processes through multidimensional population balance equations. I. A resolution algorithm based on the method of classes. *Chem Eng Sci*. 2003;58:3715–3727.
6. Hounslow MJ, Pearson JMK, Instone T. Tracer studies of high-shear granulation. II. Population balance modelling. *AIChE J*. 2001;47: 1984–1999.
7. Verkoeijen D, Pouw GA, Meesters GMH, Scarlett B. Population balances for particulate processes—a volume approach. *Chem Eng Sci*. 2002;57:2287–2303.
8. Scarlett B. Particle populations—to balance or not to balance. *Powder Technol*. 2002;125:1–4.
9. Iveson SM. Limitations of one-dimensional population balance models of wet granulation processes. *Powder Technol*. 2002;124:219–229.
10. Rippin DWT. Statistical methods for experimental planning in chemical engineering. *Comput. Chem. Engng*. 1988;12:109–116.
11. Bard Y. *Nonlinear Parameter Estimation*. New York: Academic Press, 1974.
12. Clerin P, Laurent V. Alumina particle breakage in attrition test. *Light Metals*. 2001:41–47.
13. Gwyn JE. On the particle size distribution function and the attrition of cracking catalysts-laboratory studies. *AIChE J*. 1969;15:35–39.
14. Bemrose CR, Bridgewater J. A review of attrition and attrition test methods. *Powder Technol*. 1987;49:97–126.
15. Boerefijn R, Gudde NJ, Ghadiri M. A review of attrition of fluid cracking catalyst particles. *Adv Powder Technol*. 2000;11:145–174.
16. Wachtman JB. *Mechanical Properties of Ceramics*. New York: Wiley, 1996.
17. Shah BH, Ramkrishna D. A population balance model for mass transfer in lean liquid–liquid dispersions. *Chem Eng Sci*. 1973;28: 389–399.
18. Haseltine EL, Patience DB, Rawlings JB. On the stochastic simulation of particulate systems. *Chem Eng Sci*. 2005;60:2627–2641.
19. Bilgili E, Hamey R, Zhupanska O, Scarlett B. Nano-grinding of pigment aggregates using a wet stirred media mill: elucidation of the kinetics and breakage mechanisms. Proceedings of 2nd International conference on population balance modelling. Valencia, Spain, May 5–7; 2004:33–36.
20. Kostoglou M, Karabelas AJ. A study of the nonlinear breakage equation: analytical and asymptotic solutions. *J Phys A: Math Gen*. 2000;33:1221–1232.
21. Epstein B. Lognormal distributions in the breakage of solids. *Ind Chem Eng*. 1948;41:2289–2291.
22. Hill PJ, Ng KM. Statistics of multiple particle breakage. *AIChE J*. 1996;42:1600–1611.
23. The Mathworks Inc. MATLAB user's guide. Natick, MA, 2000.
24. Finlayson BA. *Nonlinear Analysis in Chemical Engineering*. New York: McGraw-Hill, 1980.
25. Kumar S, Ramkrishna D. On the solution of population balance equations by discretization-III. Nucleation, growth and aggregation of particles. *Chem Eng Sci*. 1997;52:4659–4679.
26. Ma DL, Tafti DK, Braatz RD. High-resolution simulation of multidimensional crystal growth. *Ind Eng Chem Res*. 2002;41:6217–6223.
27. Gardner RP, Sukanjnajtee K. A combined tracer and back-calculation method for determining particle breakage functions in ball milling. I. Rationale and description of the proposed method. *Powder Technol*. 1972;6:65–74.
28. Witkowski WR, Miller SM, Rawlings JB. Light scattering measurements to estimate kinetic parameters of crystallization. In: Myerson AS, Toyokura K, editors. *Crystallization as a separations process*. Washington: ACS, 1990:102–114.
29. The Math Works, Inc. Optimization Toolbox User's Guide, Natick: The Math Works, 2006.
30. Whittington B, Ilievski D. Determination of the gibbsite dehydration reaction pathway at conditions relevant to Bayer Refineries. *Chem Eng J*. 2004;98:89–97.
31. Forsythe WL, Hertwig WR. Attrition characteristics of fluid cracking catalysts—laboratory studies. *Ind Eng Chem*. 1949;41:1200–1206.

Manuscript received Apr. 28, 2006, and revision received Jan. 9, 2007.